Analysis of Low Level Wind Shear Flight Perturbations on Final Approach Using QAR Data

Sérgio Vasco Guerra de Sousa Silva
sergio.silva@tecnico.ulisboa.pt

Instituto Superior Técnico, Universidade de Lisboa, Portugal

October 2022

Abstract

The final stages of approach to landing are a critical part of the flight of an aircraft. This phase of flight is characterized by low speed and proximity to the ground, with minimal levels of energy, thus rendering the aircraft vulnerable to atmospheric perturbations and in greater danger of uncontrolled ground contact. The low level wind shear and turbulence are quasi-stochastic phenomena that introduce difficulties on the flight path control of landing aircraft and must be considered in the interest of safety. Due to local weather patterns and terrain configuration, one particular case were these atmospheric phenomena play an important role and impose operational limitations is the Madeira International Airport. Using aircraft data from Quick Access Recorders in conjunction with surface wind at Madeira Airport, some key aircraft parameters and reactions are analyzed in correlation to surface wind. Data cleaning, filtering and smoothing is described, particularly by the use of a Rauch-Tung-Striebel algorithm, as well as side slip angle estimation and calibration of data from angle-of-attack sensors for overall data coherence. Spot wind vector components are extracted from QAR data, and various turbulence and flight hazard metrics are analyzed considering the wind conditions, including the achievement of stabilization criteria, a standard practice in air transport industry. Considering a specific surface wind direction at the touchdown point, no definitive geospatial correlation could be found between flight perturbations and wind conditions except the increase of stochastic turbulence connected with higher surface wind intensities.

Keywords: Windshear, QAR, Rauch-Tung-Striebel, Turbulence, Madeira Airport

Abbreviations

AAL – Above Airdrome Level
AOA – Angle of Attack
EASA – European Aeronautical Safety Agency
FAA – Federal Aviation Administration
FDM – Flight Data Monitoring
ILS – Instrument Landing System
PAPI – Precision Approach Path Indicator
QAR – Quick Access Recorder
RNP (AR) – Required Navigation Performance (Authorization Required)
TSO – Technical Specification Order
VOR – Very High Frequency Omnidirectional Range
WMO – World Meteorological Organization

Nomenclature

x, y, z – Positions
X, Y, Z - Forces along x, y, z
u, v, w - Velocities along x, y, z
p, q, r - Angular rates around x, y, z
C_L, C_D - Coefficient of Lift, Drag
θ, ϕ, ψ - Angles of pitch, roll and heading
α, β - Angle of attack, sideslip
γ, χ - Flight path angle, Track angle
φ, λ - Latitude, Longitude
b, A, S – Wing span, Aspect ratio, Area
$c, \bar{c}, \Lambda$ – Wing chord, Mean chord, Sweep
$C_{l_\alpha}, C_{L_\alpha}$ - Gradient of C_L with α: 2d airfoil, 3d wing
Q - Dynamic pressure ($\frac{1}{2}\rho V^2$)
W – Wind speed
g – Gravitic acceleration
V – Aircraft True Air Speed
Subscripts
i – Inertial (earth) frame
b – Body frame
a – Air mass frame (wind)

1 Introduction

Both turbulence and wind shear introduce challenges on the maintenance of adequate speed, flight path and general aircraft control. In this paper, the first is understood as a stochastic process whereby considering a sufficient distance, the integral of all movements of air mass tend to cancel out, while the latter results in a permanent and relatively sudden, shift in direction and or velocity of the wind.

At Madeira, the conjunction of runway location, orographic features and the prevailing wind direction makes this airport prone for turbulence and wind shear phenomena, making it notorious for its challenging approaches even on moderate winds. To mitigate the operational risk, a set of measures have been implemented including the enforcement of sectorial wind limits above which the operation is forbidden[1]. These limits have been established in the 1970's and, albeit some minor revisions, are still in force since there is no solid evidence that these could be relaxed while keeping the desired level of safety.

In the first 100 days of 2018 around 550 movements and 80 000 passengers have been affected by flight delays or cancellations due to wind conditions, with the corresponding economic impact [2]. This loss has prompted the authorities throughout the years to promote a number of studies regarding the wind flow around the airport. Thus far, to the knowledge of the author, none has included the use aircraft flight recorder data to measure quantitatively the flight perturbations introduced on the approach phase.

All modern turbine powered aircraft with a Maximum Take-off Mass above 5 700kg are required by regulations to carry on board a Flight Data Recorder (FDR) which record many key parameters[3] that are available for download and analysis after flight. This data is routinely exploited by the airlines under Flight Data Monitoring (FDM) programs whose main objective is to monitor the safety of operations.

This study is based on data pertaining to A320 family of aircraft which is the most common type of aircraft at Madeira International Airport representing over 50% of all movements [4]. The flight phase analyzed is the approach segment from 300' AAL (Above Airdrome Level) until touchdown, as it is the portion where flight perturbations represent the most hazard.

It is plausible that the type and strength of low-level windshear and turbulence is dependent on geographic location, altitude, wind direction and intensity. The main purpose of this work is to establish a data processing methodology and establish a proof of concept. To contain the greatest number of variables, only the approaches to runway 05 and wind from direction of 350° (± 5º) magnetic are considered.

1.1 Previous Work and State of the Art

The exploitation of QAR data poses a number of challenges because it is affected by problems of sensor bias, inaccuracy, low sample rates and desynchronization. Haverdings and Chan[5] give an approach to the data processing using a Kalman filter-smoother, calibration of sensors by multiple regression analysis and clues to parameter extraction. Höhndorf *et al*[6] worked on techniques for the reconstruction of aircraft states during approach and landing by using a Rauch-Tung-Striebel filter-smoother and proposed some sensible values for the covariance matrices to be used. Additionally, a method of parameter estimation is employed by Sembiring et al[7] which allows for a correction of bias/systemic errors and better accuracy. Also, Huang et al[8] provide a method for vertical wind component extraction from the available QAR data as well as AOA calibration.

On the effects of wind shear on approach most body of work is condensed by ICAO on its Doc 9817[9] where all the major aspects of Low Level Wind shear are treated. Also the EASA and FAA criteria for Airborne wind shear warning and escape guidance systems for transport airplanes is presented, as determined on TSO-C117a[10]. This criteria is based on a denominated F-factor which was first proposed by Bowles[11] and reflects the aircraft's rate of change of the energy state over a certain period of time.

On the subject of acceptable flight perturbations during final approach, extensive work on metrics and criteria has been developed since 1970's by NASA Ames and Langley Research Centers in connection to the study of Wake Vortex Encounter or wind shear, but no definite industry or scientific consensus has been established[6],[7],[14],[15]. Sammonds and Stinnett [12] proposed a maximum bank angle and roll acceleration dependent on altitude.

1.2 Paper Layout.

Firstly, an overview of the operational conditions and weather environment at Madeira Airport are presented, then, a description is made of the data filtering, smoothing, calibration and validation techniques used, most notably the use of the Rausch-Tung-Striebel method.
A description is also made on the geospatial positioning adjustments for the overall coherence of the flight path, on the angle-of-attack sensor data calibration and on the method of estimation of side slip angle.
From this processed data the 3D wind components are estimated. Based on these and vertical accelerations, some turbulence metrics are analyzed as well as hazard metrics.

2 Background

2.1 Madeira International Airport

Madeira airport is located on the southwest coast of the island, at an altitude of 51 m (191') featuring a single runway of 2481 x 45 m, with the designation 05/23.

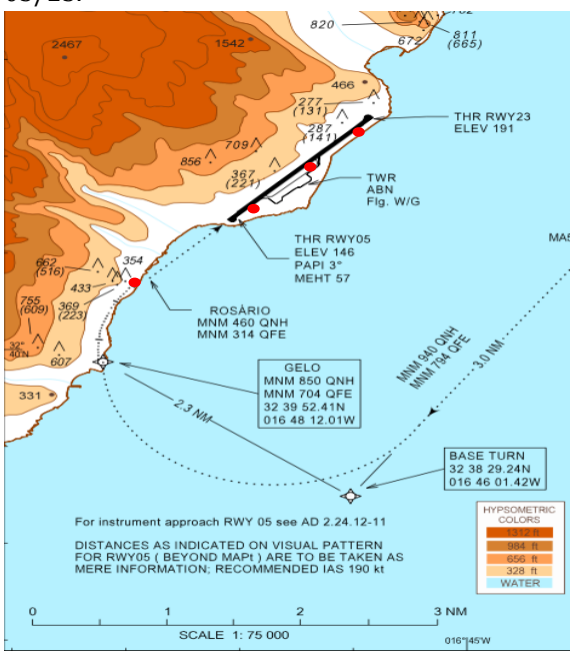

Figure 2.1 - Airport framing with surrounding terrain showing the path of curved approach to runway 05 (dotted line) and position of anemometers (red dots)[1].

The runway environment is characterized by the upwards steep inclines to the NW and downwards on other directions (see Figure 2.1) and is often affected by the turbulence of wake caused by synoptic winds [16]

Due to terrain altimetry most approaches are completed through a *circling approach* and landing on runway 05 by flying a curved path with final line-up at about 1 nm from threshold. On the vertical plane, a nominal 3° glide is indicated by PAPI.
A network of four *Vaisala Windset WA15* comprised each of an anemometer and a wind vane are installed on the airport. These sensors record at 10 sec interval the instantaneous intensity and direction of wind. See Figure 2.1

2.2 Operational Limitations

There are different wind limitations for take-off and landing, the latter being more restrictive and most affecting the operation. These limits are generally referred to the touchdown point anemometer, with the direction and intensity being averaged over 2 minutes and the 'gust' is the maximum intensity in the same 2 minutes.

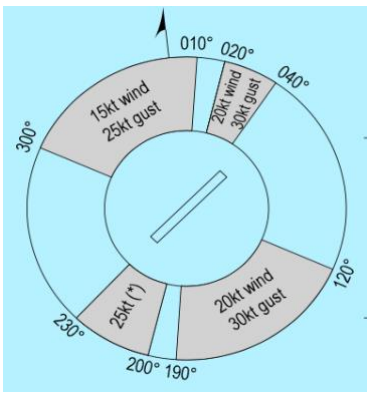

Figure 2.2 - Sectorial wind limitations for landing at Madeira in 2022 [1].

2.3 Aircraft

The aircraft used as source of data are the Airbus A319, A320 and A321 which differ mainly on fuselage length and maximum masses, being otherwise very similar. These have fly-by-wire controls with several features of flight stabilization with a more benign set of flight characteristics than conventionally controlled aircraft. Nevertheless, this is far from eliminating perturbations induced by turbulence or windshear.

2.4 'Stabilized Approach' concept

An air transport industry agreed safety standard is the stabilized approach concept. This amounts generically to the attainment and conservation of certain key parameters (airspeed, pitch, roll, thrust, configuration) in a defined range during the last stages of the approach – typically bellow 1000', with

some parameters allowed to stabilize as low as 500' AAL, until touchdown. Although these criteria are designed for the most common straight-in approach, it is still applicable to this special case of curved approach, albeit some adaptations. These are used as reference further ahead.

3 Data Gathering and Preprocessing

3.1 Meteorological Data

For this study only the direction of 350°±5° magnetic at the threshold of runway 05 anemometer was chosen for analysis because it is known to cause challenges on aircraft control during approach and it is at the heart of the most restrictive sector. In terms of meteorological reporting, the wind that the ATC must report to aircraft before landing is a 2 minute average. For this reason, only flights that present the relevant average wind direction during the last 2 minutes before touchdown are analyzed, amounting to 161 datasets.

3.2 Preprocessing

To take advantage of most data, an approach of 'upsampling' all parameters to 4Hz is taken. Depending on the type of parameter, the perceived quality of data and the dependence of posterior analysis, different methods of interpolation with respect to time are used: Linear is used on parameters that change slowly; Cubic for parameters with dynamic or oscillatory behavior or angular representation.

In the case of the positional coordinate system (Latitude, Longitude, Altitude), it is converted to a local orthogonal isometric cartesian system with origin conveniently located on the threshold of runway 05, with x pointing East, y pointing North and z pointing up.

This conversion is made using the WGS84 ellipsoid (the same used on aircraft navigation systems).

3.2.1 Rauch-Tung-Striebel (RTS) Smoother

The RTS smoother is used as a method to estimate the most probable state of a dynamic system and its covariance at a given time having in consideration all the measurements, both past and future. For this reason, this algorithm is only possible to implement on already existing datasets. It is applied in a two-stage process: The first, consists in applying a Kalman filter to data in a forward-time manner, saving the filter output at each step; The second stage is a time-reverse pass whereby the algorithm incorporates its knowledge of the 'future' into 'past' measurements. In this sense, unlike low-pass filters, the RTS is able to behave optimally and not remove real variations along with noise[17]. The filter is applied with discrete time steps ($\Delta t = 0.25\ s$) running through a prediction, measurement, and update cyclical process. The following equations in vectorial form describe the process.

Taking $\hat{\boldsymbol{x}}$ as the predicted state vector, $\boldsymbol{F}$ as the transition state function, $\boldsymbol{B}$ as the input function and $\boldsymbol{u}$ as the input vector, one can predict the state at instant t by

$$\hat{\boldsymbol{x}}_{t|t-1} = \boldsymbol{F}_t \hat{\boldsymbol{x}}_{t-1|t-1} + \boldsymbol{B}_t \boldsymbol{u}_t \quad (1)$$

The state covariance $\boldsymbol{P}$ is a function of the same parameter at the previous epoch plus the process covariance $\boldsymbol{Q}$

$$\boldsymbol{P}_{t|t-1} = \boldsymbol{F}_t \boldsymbol{P}_{t-1|t-1} \boldsymbol{F}_t^T + \boldsymbol{Q}_t \quad (2)$$

Now the prediction can be updated by the measurement $\boldsymbol{z}$, using a measurement function $\boldsymbol{H}$. For this, the residual $\boldsymbol{y}$ between the prediction and the measurement will be calculated first

$$\boldsymbol{y}_t = \boldsymbol{z}_t - \boldsymbol{H}_t \hat{\boldsymbol{x}}_{t|t-1} \quad (3)$$

the Kalman gain $\boldsymbol{K}$ is found by the next expression, where $\boldsymbol{R}$ is the measurement noise covariance

$$\boldsymbol{K}_t = \boldsymbol{P}_{t|t-1} \boldsymbol{H}_t^T (\boldsymbol{H}_t \boldsymbol{P}_{t|t-1} \boldsymbol{H}_t^T + \boldsymbol{R}_t)^{-1} \quad (4)$$

and the state vector and its covariance are updated and will be used as the starting point for the next epoch

$$\hat{\boldsymbol{x}}_{t|t} = \hat{\boldsymbol{x}}_{t|t-1} + \boldsymbol{K}_t \boldsymbol{y}_t \quad (5)$$

$$\boldsymbol{P}_{t|t} = (I - \boldsymbol{K}_t \boldsymbol{H}_t\ ) + \boldsymbol{P}_{t|t-1} \quad (6)$$

After the Kalman filter is run, the RTS smoother will run 'backwards' in time.

$$\boldsymbol{P}_t^{RTS} = \boldsymbol{F}_t \boldsymbol{P}_t \boldsymbol{F}_t^T + \boldsymbol{Q}_t \quad (7)$$

$$\boldsymbol{K}_t = \boldsymbol{P}_t \boldsymbol{F}_t^T \boldsymbol{P}_t^{RTS^{-1}} \quad (8)$$

$$\hat{\boldsymbol{x}}_t = \hat{\boldsymbol{x}}_t + \boldsymbol{K}_t (\boldsymbol{x}_{t+1} - \boldsymbol{F}_t \hat{\boldsymbol{x}}_t) \quad (9)$$

$$\boldsymbol{P}_t = \boldsymbol{P}_t + \boldsymbol{K}_t (\boldsymbol{P}_{t+1} - \boldsymbol{P}_t^{RTS}) \boldsymbol{K}_t^T \quad (10)$$

The use of the RTS filter smoother allows for several sources of data to be incorporated in the best estimation of the parameters through the manipulation of the measurement function $\boldsymbol{H}$ and the noise covariance of the measurements, $\boldsymbol{R}$. A mix of Inertial, barometric and GPS data was used for the estimation of Position, Velocity and Acceleration, all in x, y, and z.

An additional advantage is that the extracted parameters tend to converge to a state of coherence among themselves as they are related with each other through the transition state function $\boldsymbol{F}$ and

after the update step, sensor bias tends to be cancelled out for the next iteration.

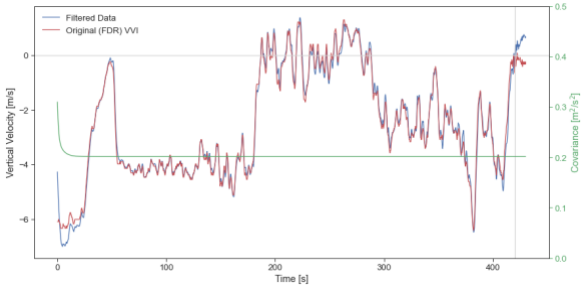

Figure 3.1 - A sample of Vertical Velocity data from a flight. After the first few iterations the filtered data converges with measured data and the covariance stabilizes and maintains constant throughout the process.

3.2.2 Trajectory shift / adjustment

Due to imprecision on aircraft navigation system and/or difference of datum the geospatial data evidenced dispersion among samples and some degree of offset from the runway. This offset was corrected by shifting the flight path data so that it is made to intersect two conveniently selected points, one on the runway centerline and other on the exit taxiway.

Figure 3.2 – Example of the horizontal projection of the flight path after RTS smoothing and adjustment. The points referenced are used for Local Coordinate System origin (Threshold 05) and trajectory shifting (Touchdown and Taxiway)[Image source: Google Earth®].

In this manner the trajectory is corrected laterally and longitudinally relative to the runway. Once the horizontal offsets are applied, it is recovered where, along the runway, did the touchdown take place. This is important because the runway has an upslope so the altitude of touchdown increases along the runway. Once the touch down vertical offset is determined, that correction is applied to all altitudes.

4 Data analysis

4.1 3D Wind Estimation

A tridimensional wind estimation is not computed on board the aircraft, but it is important to know the vertical component of the wind to calculate parameters such as turbulence and wind shear metrics. A method of estimating the complete wind vector can be implemented by realizing that the wind is the difference between the aircraft inertial velocity and its velocity relative to the air mass.

$$\boldsymbol{V}_{ai} = \boldsymbol{V}_{bi} - [\boldsymbol{T}_{ib}] \cdot \boldsymbol{V}_{ab} \qquad (11)$$

The body velocity relative to the inertial frame V_{bi} was computed in the RTS smoother. The velocity relative to air mass expressed in body frame is

$$\boldsymbol{V}_{ab} = \begin{bmatrix} V_a \cos\alpha \cos\beta \\ V_a \cos\alpha \sin\beta \\ V_a \sin\alpha \end{bmatrix} \qquad (12)$$

Where V_a is the velocity relative to the air expressed in wind axes, available in the FDR as True Airspeed.

The body angles ψ, θ and ϕ are available on QAR data and have been subject to smoothing as described in 3.2.1. The sideslip β is not available on QAR although it can be estimated from the record of lateral accelerations. The Angle of Attack, α is available in the data, but it is known that these values need a calibration before use as they present bias and scaling errors.[5], [8]

4.1.1 Angle of Attack Calibration

The fact that the AOA probes are in the forward section of the fuselage affects the measurements when the aircraft is rotating about its y axis (pitching).

The method of correction proposed is through the relation [8]:

$$\frac{\theta - \gamma}{\cos\phi} = k\left(\frac{AOAL + AOAR}{2} - \frac{Lq}{V_a}\right) + c \qquad (13)$$

Where $AOAL$ and $AOAR$ are the values on the QAR of the left and right AOA probes, and V_{ba} is the true air speed and L is the arm length from the center of gravity of the aircraft to the AOA probes. The constants k and c are the resultant of a least squares fit of the above expression over a flight data.

Inherent to this method of AOA correction is the assumption that the integral of the wind's vertical component throughout the considered flight path is zero, otherwise γ is erroneous.

4.1.2 Sideslip angle estimation

The aircraft is not equipped with sensors for the sideslip angle β. The proxy measure used to estimate β is the lateral acceleration and a method has been suggested by Haverdings and Chan [18]. This method, with adaptations, recognizes that on a sideslip there are two major contributors to side forces: the vertical fin and the fuselage.

$$Y = Y_{vfin} + Y_{fus} \qquad (14)$$

Taking the vertical fin as a semi-wing of symmetrical profile and the fuselage as a cylindrical body subject to transverse flow, this expression can be rearranged and solved for β

$$S_{fus} C_{D_{fus}} \beta^2 + S_{vfin} \frac{\partial C_{l_{fin}}}{\partial \beta} \beta - \frac{m a_y}{Q} = 0 \qquad (15)$$

4.2 Model validation

Although there is no information about the wind affecting the aircraft other than that derived by the aircraft systems themselves, it can nevertheless be verified if the method of filtering and processing the data produces results that are in general agreement with aircraft sensors.

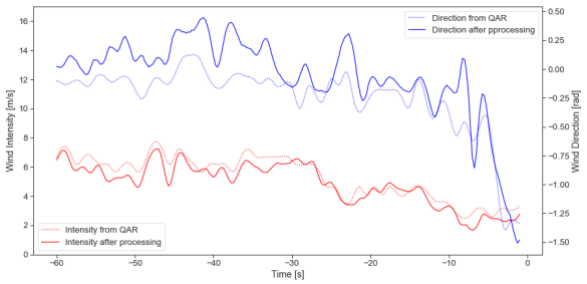

Figure 4.1 - Sample of wind values for a particular flight as recorded by QAR and after data processing.

4.3 Wind Categorization

Wind behavior studies by Wieringa[19] shows that the gustiness may be attributable to many phenomena but a near linear relation can be established with mean wind intensity, which was verified for the flights being considered. Generally, the intensity varies between 0.6 and 1.4 of the mean value while the direction varies between ±40° (see Figure 4.2 (b)). Wieringa notes also that small scale wind fluctuations have negligible correlation in locations further away than 100 m downwind or 50 m crosswind from the observation point - Only mean intensity and general gustiness, when averaged over a sufficiently long period, are correlatable.

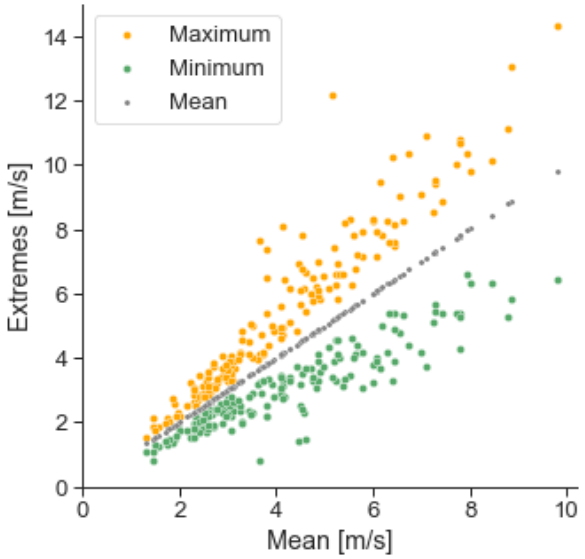

Figure 4.2 – (a) Maximum and minimum of the wind intensity during the 2 minutes before touchdown, for each flight.

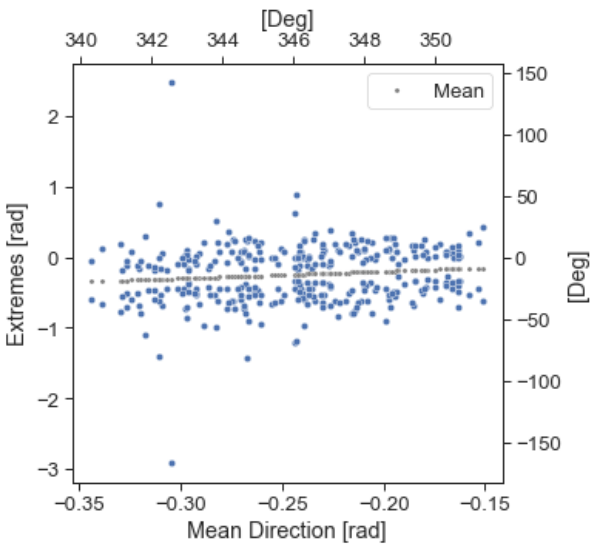

Figure 4.3 - Maximum and minimum directions of the same samples.

For this reason, as will be seen ahead, it is difficult to find a direct correlation between specific aircraft flight perturbations and surface wind variations, but rather a general connection between mean surface wind intensity and gustiness.

Bearing in mind this correlation, it was selected to conduct the analysis of the aircraft parameters during the approach by using a division into 4 classes of surface wind. These are based on the 2 minute mean intensity at the Rwy 05 anemometer, as shown on Table 1.

Table 1- Wind Class division

Wind Class	Lower bound	Higher bound	# Samples
1	0 m/s	4 m/s	86
	0 kts	7.8 kts	
2	4 m/s	5.5 m/s	38
	7.8 kts	10.7 kts	
3	5.5 m/s	7 m/s	23
	10.7 kts	13.6 kts	
4	> 7 m/s	-	15
	> 13.6 kts	-	

4.4 3D Wind Component results

The wind components extracted show mainly a stochastic behavior represented by the wide bands of the standard deviation. For all wind classes the crosswind is maximum between -800 m and -500 m, then reducing progressively until touchdown, except for class 4, where a trend inversion is felt momentarily just before crossing the threshold. This crosswind reduction is significant as it forces the pilot to correct the lateral axis by using bank on a late stage and may unstabilize the approach laterally.

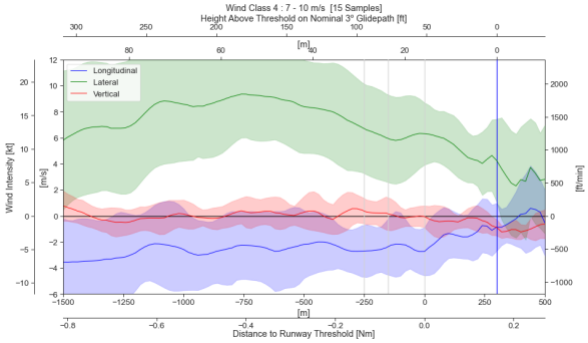

Figure 4.4 - Mean wind components class 4 wind. Shaded areas represent a Standard Deviation. Positive directions are forward, right and up.

It was observed after charting the aircraft path that there is a significant geospatial dispersion up until 500 m distance from threshold. This means that for exact same surface wind conditions, two aircraft on slightly different paths may observe different local winds.

Figure 4.5 - Geospatial dispersion of Flights analyzed. [Base image © Google Earth]

5 Flight perturbations on final

5.1 Vertical Acceleration Turbulence Metric

The simplest expression of turbulence can be measured by the variation of vertical acceleration which is a function of several factors, namely the weight, velocity, altitude and the nature of the turbulence, making this metric very aircraft-specific. Although it is difficult to decouple the intentional aircraft maneuver from the turbulent inputs, in the case of this analysis, since the aircraft are of the same type and share very similar characteristics, is seems adequate to use the metric of vertical acceleration to quantify and compare the disturbances among them.

For the classification of turbulence according to this metric, the table proposed on reference [20] may be used. See Table 2.

Table 2 - Turbulence categorization based on vertical acceleration [20]

Category	Peak Accel. (Δn)
None	|Δn| < 0.15 g
Light	0.15 g ≤ |Δn| < 0.5 g
Moderate	0.5 g ≤ |Δn| <1.0 g
Severe	|Δn| ≥ 1.0 g

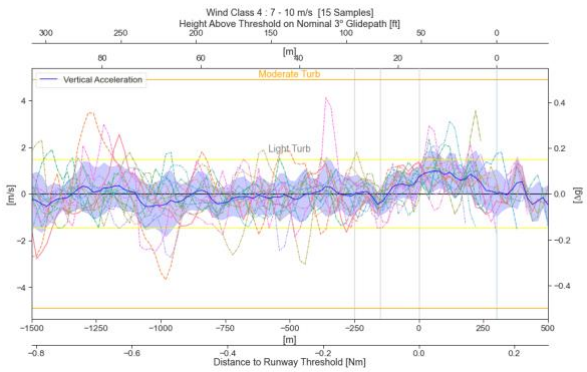

Figure 5.1 - Vertical Acceleration for class 4 winds. The blue band represents one Standard Deviation.

From Figure 5.1 it can be observed that effectively the vertical acceleration amplitude on wind class 4 only occasionally approaches the medium but it must be noted that at this stage, the aircraft is flying at a speed of $1.3 \cdot V_S$, so the maximum load factor possible is on the order of $1.3^2 \approx 1.7$. Reaching a Δn of 0.5 (moderate turbulence) would mean at this late stage of the approach, a situation dangerously close to stall but also would imply a change in vertical trajectory that most probably would prompt the pilot to initiate a Go-Around maneuver.

5.2 Wind shear phenomena and hazard metrics F-Factor

The F-factor, loosely translates the remaining capability of an aircraft to climb away from the ground in the presence of shear. It can be expressed as

$$F = \frac{\dot{U}_x}{g} - \frac{w}{V} \qquad (16)$$

It must be noted that a negative F corresponds to a performance increasing windshear, such as the reduction of tailwind or an updraft.

This factor, when applied on a given instant may result in very large values for F, which are usually associated with atmospheric turbulence. For a significant defect in performance to develop, a sufficiently large time must be considered in the application of the F-factor.

From the work of Lewis *et al* [21] it can be concluded that for a twin-engine on approach, the lowest $\bar{F}$ is 0.14 over a distance of 600m – which is roughly the distance covered in 10 seconds by an aircraft at approach speeds.

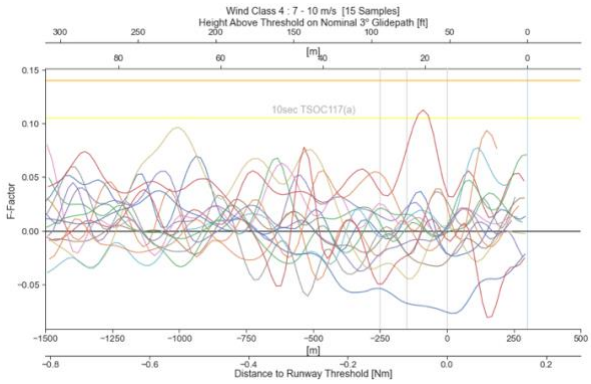

Figure 5.2 - F-factor average calculated over 10" for flights wind class 4. The yellow line represents the FAA TSO-C117(a) criteria for alert.

On the analysis of Figure 5.2 it worth noting the relatively large $\bar{F}$, particularly on the last 500 m to touchdown. Although the positive $\bar{F}$ are the performance degrading and hence the most dangerous, it must not be discounted the destabilizing effect of negative $\bar{F}$ at such late stage of the approach, possibly causing an overshoot of the landing point and adding unwanted energy to the aircraft causing a long landing.

On the positive $\bar{F}$ cases (deteriorating performance), it must be considered that bellow a height of 200 ft any marked energy loss leaves the pilot little time for recovery and the risk of firm or uncontrolled ground contact is substantial. In this late stage of approach the alert level for $\bar{F}$ might be inappropriate.

5.3 Bank Angle

Simmonds et al [22] proposed the bank angle as means to define acceptable conditions following a disturbance by wake vortex encounter. It is appropriate to use the same metrics for turbulence induced roll as the situation does not differ significantly – both scenarios encompass an uncommanded aircraft movement at low altitudes. In order to compare and have a notion of the bank angles reached during the approach to runway 05, the bank histories for wind class 3 were plotted on Figure 5.3 below.

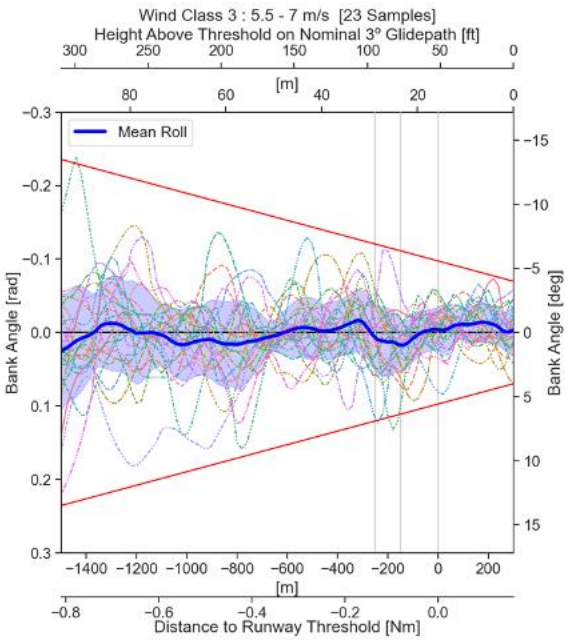

Figure 5.3 - Roll histories for wind class 4. The red straight lines represent the roll hazard criteria proposed by Simmonds et al. The blue band represents one Standard Deviation.

Note that it is not possible to determine if the bank was caused by turbulence or pilot command or a blend. Either way, it is recognized that while most of

the flights remain inside the hazard criteria, there are a few that go out but from the inspection of Figure 4.5 it can be observed that a significant number of flights have a late lineup and consequently induce a right bank exceedance; On the other hand, a left bank exceedance is very seldom the case. It can be observed on all wind classes that up until 1000m from the threshold there is a skew to the right.

For the higher wind classes, the bank angle dispersion is larger, visible also by the width of the Standard Deviation bands. This is expected due to the increased turbulence.

5.4 Vertical speed

As per the stabilization criteria mentioned on section 2.3, the vertical speed during approach should not exceed -1000 ft/min [≈-5 m/s]. For this type of visual approach and while initially adjusting to intercept the PAPI glidepath it is natural that for a short period of time some exceedance is observed. After being stabilized on the glide, it is not expected to see such exceedances except for very short spikes, due to turbulence perturbation and/or momentary adjustment.

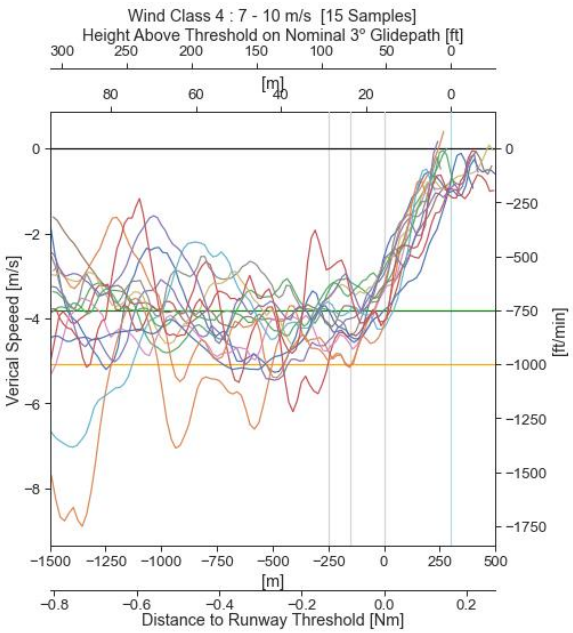

Figure 5.4 - Vertical speed during approach for the class 4 wind. The gren line represents the normal rate of descent and the orange line the 'alert' limit of 1000'/min.

It is was generally noticeable that for higher classes of wind the amplitude and hence the dispersion of vertical speeds is higher.

5.5 Speed Control

The speed interval commonly accepted in the stabilization criteria is the target approach speed +10/-5 kts. It is clear on Figure 5.5 the dispersion is significant but note that occasionally there are exceedances on the fast side but there is none on the slow side. This is justifiable because on strong and gusty conditions pilots tend to prefer to fly faster to avoid the risk of stall due to a sudden lack of wind.

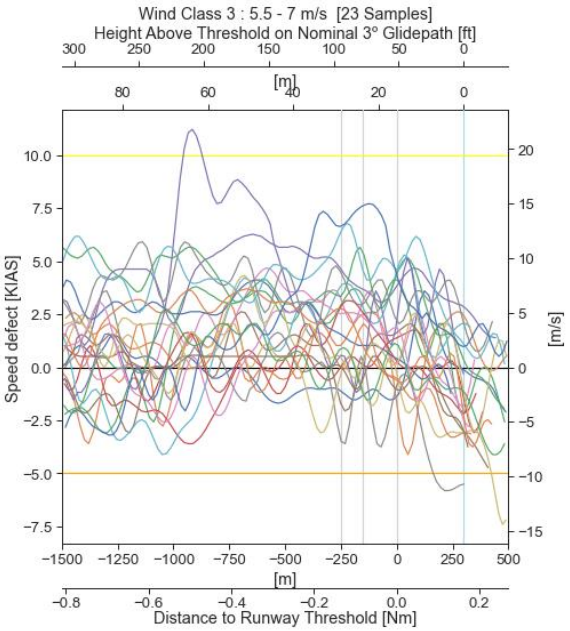

Figure 5.5 - Speed defect during approach for class 3 wind.

5.6 Vertical acceleration at touchdown

The purpose of this analysis is to evaluate if the increasing surface wind intensity would correlate to heavier touchdowns. A touchdown should not exceed a normal load factor of 1.8g. It can be seen from Figure 5.6 that there is no correlation of wind intensity with the normal load factor.

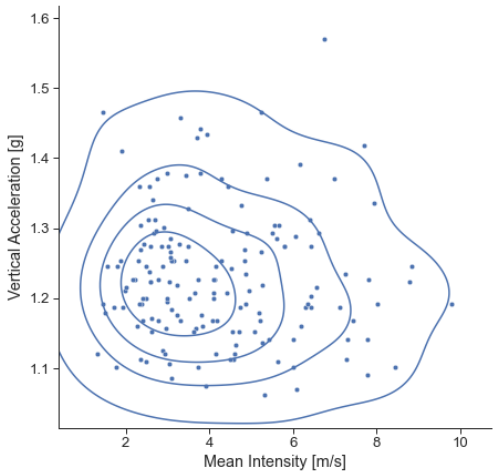

Figure 5.6 - Vertical Load factor at touchdown.

6 Conclusion

Madeira Airport wind regime continues to deserve a more profound study as just a small advance is made through this present approach.

It is of paramount importance that great attention is dedicated to the filtering, calibration and matching of data so that the dataset has the coherence necessary for posterior analysis. On the assurance of compatibility of data, the use of the Rauch-Tung-Striebel filter smoother proved very robust in delivering coherent interpolation and adjustment to raw sensor measurements and was particularly useful on the flight path recreation.

As for the wind regimes and their impact on the operation, it was not evident the existence of a strong correlation between the prevailing mean wind direction/intensity and a pattern of winds at specific points along the approach path. Rather, the stochastic nature of wind suggests that intermittent local phenomena are responsible for the sudden variation of airflow and consequent aircraft disturbance. Such conclusion is also suggested by the turbulence analysis.

The adaptation of the F-factor to present conditions showed that occasionally some flights suffer a late change of its energy level, but further investigation should be made to ascertain the validity of this metric at such late stage of approach.

The analysis of aircraft stabilization criteria showed generally that greater dispersion of parameters is to be expected in connection with greater wind intensities, but no clear pattern was detected in relation to other parameters.

Acknowledgements

The author would like to thank Prof. Afzal Suleman for the support and counseling.

References

[1] NAV Portugal E.P.E., "AIP Portugal." p. LP_AD_2_LPMA, 2021.

[2] *Resolução da Assembleia Legislativa da Região Autónoma da Madeira n.o 26/2018/M*. 2018, pp. 4–5.

[3] EASA, "CS-25 Easy Access Rules for Large Aeroplanes," 2021, [Online]. Available: https://www.easa.europa.eu/document-library/general-publications/easy-access-rules-large-aeroplanes-cs-25.

[4] ANAC, "Boletim Estatístico Trimestral Nº44, 4º trimestre 2019," 2020.

[5] H. Haverdings and P. W. Chan, "Quick Access Recorder Data Analysis Software for Windshear and Turbulence Studies," *J. Aircr.*, vol. 47, no. 4, pp. 1443–1447, Jul. 2010, doi: 10.2514/1.46954.

[6] L. Höhndorf, J. Siegel, J. Sembiring, P. Koppitz, and F. Holzapfel, "Reconstruction of aircraft states during landing based on quick access recorder data," *J. Guid. Control. Dyn.*, vol. 40, no. 9, pp. 2387–2392, 2017, doi: 10.2514/1.G002637.

[7] J. Sembiring, L. Drees, and F. Holzapfel, "Extracting unmeasured parameters based on quick access recorder data using parameter-estimation method," *AIAA Atmos. Flight Mech. Conf.*, pp. 1–12, 2013, doi: 10.2514/6.2013-4848.

[8] R. Huang, H. Sun, C. Wu, C. Wang, and B. Lu, "Estimating eddy dissipation rate with QAR flight big data," *Appl. Sci.*, vol. 9, no. 23, pp. 1–14, 2019, doi: 10.3390/app9235192.

[9] International Civil Aviation Organization, "Doc 9817 Manual on Low-level Wind Shear," 2005.

[10] FAA, "TSO-C117a, Airborne windshear warning and escape guidance systems for transport airplanes," vol. 8, no. July 1988, pp. 1–80, 1996.

[11] R. L. Bowles, "Reducing Windshear Risk Through Airborne Systems Technology," *ICAS*, pp. 1603–1630, 1990.

[12] R. I. Sammonds and G. W. Stinnett Jr, "Hazard Criteria for Wake Vortex Encounters," 1975.

[13] E. C. Hastings, G. T. Holbrook, and G. L. Keyser, "Preliminary Results of Simulated Vortex Encounters by a Twin-Engined Commercial Aircraft on Final Landing Approach," 1980.

[14] E. Stewart, "A piloted simulation study of wake turbulence on final approach," in *23rd Atmospheric Flight Mechanics Conference*, American Institute of Aeronautics and Astronautics, 1998.

[15] D. D. Vicroy *et al.*, "Characterizing the Hazard of a Wake Vortex Encounter," *AIAA*, 1997.

[16] M. Belo-pereira and J. A. Santos, "Air-Traffic Restrictions at the Madeira International Airport Due to Adverse Winds," no. July 2007, 2020.

[17] R. R. Labbe Jr, *Kalman and Bayesian Filters in Python*. 2018.

[18] H. Haverdings and P. W. Chan, "Quick Access Recorder (QAR) Data Analysis Software for Windshear and Turbulence Studies," in *1st AIAA Atmospheric and Space Environments Conference*, Jun. 2009, no. June, doi: 10.2514/6.2009-3871.

[19] J. Wieringa, "Representativeness of wind observations at airports.," *Bull. Am. Meteorol. Soc.*, vol. 61, no. 9, pp. 962–971, 1980.

[20] WMO, "Aircraft Meteorological Data Relay (AMDAR) Reference Manual," *World Meteorol. Organ. Doc. WMO-958*, 2003.

[21] M. S. Lewis, P. A. Robinson, D. A. Hinton, and R. L. Bowles, "The Relationship of an Integral Wind Shear Hazard Aircraft Performance Limitations," 1994.

[22] R. I. Simmonds, G. W. Stinnett Jr., and W. E. Larsen, "Wake Vortex Encounter Hazard Criteria for Two Aircraft Classes," 1976. doi: NASA-TM-X-73113 and FAA-RD-75-206.